Chapter 7

A Multiscale Mass-Spring Model for the Dynamic Response of VACNT Foams[6]

We present a one-dimensional, multi-scale mass-spring model to describe the response of vertically aligned carbon nanotube (VACNT) foams subjected to uniaxial, high-rate compressive deformations. The model uses mesoscopic dissipative spring elements composed of a lower level chain of asymmetric, bilateral, bi-stable elastic springs to describe the experimentally observed rate-independent stress-strain response. The model shows an excellent agreement with the experimental response of VACNT foams undergoing finite deformations and enables *in-situ* identification of the constitutive parameters at the smaller length scales. We apply the model to two cases of VACNT foams impacted at 1.75 m s^{-1} and 4.44 m s^{-1} and describe their dynamic response.

7.1 Introduction

Macro-scale carbon nanotube (CNT) foams have been synthesized from vertically aligned bundles of CNTs [37] or sponges of randomly oriented CNT fibers [55]. Their exceptional mechanical properties and energy absorption characteristics make these standalone CNT-foams excellent candidates for various applications [24] including energy absorbing/protective packaging materials for electronics and mechanical systems [37,55], structural reinforcements in composites [194] and woven fibers for bulletproof tough textiles [95]. Bulk vertically aligned carbon nanotube (VACNT) foams present a hierarchical fibrous microstructure with constituent features at various length-scales ([37], Figure 3 in [169]): the individual multi-walled carbon nanotubes (MWCNTs) have a concentric tubular configuration with several walls in the nanoscale; the MWCNTs entangle with each other to form a forest-like system in the micro scale; and the bundles of MWCNTs are aligned vertically in the mesoscale. When subjected to compressive

[6] This work was performed in collaboration with F. Fraternali. FF developed the numerical code. RT developed the model with support from FF and performed the simulations.

loadings, they exhibit distinct deformation mechanisms at different lengthscales: a foam-like compression in the macro-scale; collective sequential buckling of the aligned CNT bundles in the mesoscale; and bending and buckling of individual tubes in the micro-scale [37,166]. The bulk compression response of VACNT foams is identified by three distinct loading regimes: an initial linear regime, a plateau regime governed by progressive buckles and a final densification regime [37].

VACNT foams exhibit different mechanical responses when subjected to different loading regimes. Macroscale samples in compression exhibit a viscoelastic response when subjected to long duration stress relaxation experiments in compression [60] or when tested for creep with nano-indentation [61]. The same material exhibits rate-independent deformation mechanisms in quasistatic compression experiments [62]. However, few studies suggested dependence of VACNT foam's unloading modulus and recovery on strain rate [63,64]. In the linear dynamic regime, VACNT foams subjected to torsional mode dynamic mechanical analysis exhibited a frequency invariant dissipative response [66]. The VACNTs' storage and loss moduli were shown to be independent of frequency in uniaxial linear vibration experiments [65]. VACNT foams impacted by a striker exhibit complex rate-effects: the loading response is rate-independent whereas the unloading modulus increases with strain-rate [166]. When VACNT foams are impacted at velocities higher than a critical velocity (~6.5 m s^{-1}), they support shock formation [166].

Several models have been proposed to describe the rate-independent mechanical response of VACNT foams in the quasistatic regime. Analytical micromechanical models supported by finite element models have been used to describe the response of forests of VACNTs subjected to nanoindentation with a spherical indenter [195]. It has been shown that the indentation force during nanoindentation scales linearly with tube areal density, tube moment of inertia, tube modulus and indenter radius, whereas the force scales inversely with the square of tube length [195]. Buckle formation and progression in VACNT micro-pillars under quasistatic compression has been modeled using a finite element formulation of an isotropic viscoplastic solid combined with piece-wise hardening-softening-hardening function [196]. It revealed that the buckle wavelength decreases with increasing magnitude of 'negative hardening slope' and the buckle wave

amplitude increases with the increasing width of the flow strength function well [196]. It was also found that the buckles always initiated near the substrate due to the displacement constraint and sequentially progressed, even in the absence of a property gradient, along the height of the sample [196]. Recently, a Timoshenko beam model for an inelastic column in buckling has been used to predict the critical buckling stress of VACNT micro-pillars with transverse isotropy [197].

Coarse-grained molecular dynamic simulations of VACNT foams [67] have found that the frequency-independent viscoelasticity in shearing [66] arises from rapid unstable attachment/detachment among individual CNTs induced by the van der Walls forces and contributes to the constantly changing microstructure of the CNT network. This rate-independent dissipation was also described using triboelastic constitutive models and it has been shown that the increased adhesive energy significantly increased the overall stiffness of the network compared to the tension, bending and torsion stiffnesses, suggesting that the van der Walls interaction not only contributes to energy dissipation but also influences the elasticity of the network [67]. A phenomenological multiscale mass-spring model with bi-stable elements has been used to describe the rate-independent quasistatic compressive response of macro-scale VACNT foams [198]. This model also enabled *in-situ* material parameter identification in multilayered carbon nanotube arrays, and allows the accurate modeling of experimentally observed local deformations [199]. It has been extended later to describe a few experimentally observed phenomena, such as preconditioning [199], loading history and loading direction dependency [62] and permanent damage [200]. However, numerical models of high-rate, uniaxial, finite deformation of VACNT foams have not yet been developed.

Here, we propose a phenomenological mass-spring model that uses rate-independent, dissipative spring elements in association with phenomenological damping devices [201] to describe dynamic response of bulk VACNT foams. We use this model to describe the global dynamic response observed in experiments and then to identify the microscale mechanical parameters *in-situ*. In the following sections we provide a detailed description of the experimental methods and observations (Section 7.2), a detailed description of the generalized mechanical model (Section 7.3) and the application of this model to describe

the dynamic response of VACNT foams with *in-situ* parameter identification (Section 7.4).

7.2 Brief overview of experimental methods and observations

Dynamic experiments were performed on an impact testing setup using a flat plunge striker as the loading apparatus. The complete description of the experimental setup and the data analysis methodologies can be found in [169]. The VACNT foam samples were attached to a striker and launched at controlled velocities on a frictionless guide to directly impact a force sensor. A rigidly mounted force sensor recorded the transferred force-time history during impact, while a geometric moiré interferometer measured the dynamic deformation. These measurements were then used to obtain the dynamic stress-strain diagram, from which dynamic constitutive parameters were calculated. A high-speed microscopic camera was used for *in-situ* visualization and characterization of the micro-scale complex deformations [169].

When a VACNT foam sample is impacted, the stress rises nonlinearly with strain up to the peak stress, corresponding to the maximum strain. In unloading, the stress decreases rapidly within the first 10% of the unloading strain, and gradually reaches zero. The stress-strain hysteresis loop formed by the loading-unloading cycle represents the energy dissipated during the dynamic compression. *In-situ* visualization using a high-speed microscopic camera revealed formation and progression of sequential buckle instabilities in the sample during the loading phase (see Supplementary Video 3.1). The synthesis of VACNT foams, achieved using a chemical vapor deposition (CVD) process, induces an intrinsic density gradient along the height of the samples [37,146]. Synchrotron X-ray scattering and mass attenuation measurements showed that this intrinsic density gradient is nonlinear in a sample synthesized using a floating catalyst CVD process and presents a lower density region near the growth substrate and denser region near the free surface of the sample [166]. Because of this characteristic anisotropic microstructure, buckles always nucleate at the bottom of the soft region and progress sequentially towards the stiffer region [166]. The formation and progression of instabilities is reflected also in the dynamic stress-strain diagram and the stress-time histories, and it is evident from local

stress drops followed by local stiffening [166,169]. Upon unloading, the buckles sequentially recover [166,169]. When the samples are impacted repeatedly, with increasing impact velocity, they exhibit a preconditioning effect, which is evident from the different loading paths measured during each consecutive cycle [166]. The loading response is independent of the impact velocity, and the unloading is rate-dependent [166]. The dynamic stress-strain response of VACNT foams is similar to their response in quasistatic compression until a critical impact velocity (~6.5 m s^{-1}) is reached [166]. When the samples are impacted with striker velocities higher than the critical velocity, the formation of progressive buckles transitions into the formation and propagation of a shock [166].

Here, we model only the response of samples impacted at sub-critical velocities. We consider two samples, with similar bulk densities, that were impacted by a striker with mass 7 g at two different impact velocities: 1.75 m s^{-1} (VACNT foam-1) and 4.44 m s^{-1} (VACNT foam-2). The physical properties of the two samples are summarized in Table 7.1. Both samples exhibited full recovery of the deformation upon unloading. We use experimental force-time histories to prescribe load-histories in the model, and we calculate the dynamic responses during the time the sample is in contact with the force sensor. In the following section we present the numerical model in detail.

Table 7.1. Physical properties of the VACNT foam samples

	VACNT foam-1	VACNT foam-2
Mass (mg)	5.56	5.05
Diameter (mm)	5	5
Height (mm)	1.190	1.106
Bulk density (g cm^{-3})	0.238	0.232

7.3 Mechanical model

We use a one-dimensional, multi-scale, phenomenological model to numerically describe the dynamic response observed experimentally (and summarized in Section 7.2). The model describes the response of VACNT foams at the mesoscopic scale through the discretization of the foams into a collection of lumped masses connected by dissipative springs [198]. Each mesoscopic spring represents the continuum limit of a chain of infinitely many microscopic bi-stable elastic springs. The bi-stable springs are characterized by two stable phases (pre-buckling loading and post-buckling densification) and an intermediate unstable phase (buckling phase). The dynamic snapping of the microscopic springs and the subsequent snapping back induce hysteretic energy dissipation via "transformational plasticity" [198,202]. Our model comprises two different time scales: an external time scale, which controls the evolution of the applied loading and the response at the mesoscale; and an internal time scale, which governs the dynamic relaxation of the system at the microscale, for a fixed external time. The constitutive behavior is viscous at the micro-scale, and rate-independent at the mesoscale [198,202]. Eventually, the overall response of a CNT structure can be described through a single dissipative element (macroscopic mass-spring model, [62,203]). This multi-scale model has been previous applied to describe the quasistatic response of CNT structures [62,198–200,203]. Here, the same model is applied to describe the mechanical response of VACNT foams under high-rate loading.

We briefly summarize the analytic formulation of the model at the mesoscale, which is detailed in [198]. Let us introduce a chain of $N+1$ lumped masses $m^0 \ldots\ldots m^N$, connected by N nonlinear spring elements ($N \geq 1$). The mass m^0 is clamped at the bottom (fixed-boundary), at position $x^0=0$, and the mass m^N is free at the top (free-boundary), at position $x^N=l$. Spring 1 is at the bottom and connects masses m^0 and m^1 while spring N is at the top and connects m^N and m^{N+1}. The scalar quantity, ε^i characterizes the total strain at the i^{th} spring.

$$\varepsilon^i = \frac{u^{i-1} - u^i}{h^i}, \tag{7.1}$$

where u^i is the axial displacement of the mass m^i relative to its initial position and $h^i=x^i-x^{i-1}$. The constitutive equations for each mesoscopic spring are:

$$\sigma^i = \begin{cases} \sigma^{(a,i)} = k_0^i \varepsilon^i/(1-\varepsilon^i), \text{ for } (\varepsilon^i < \hat{\varepsilon}_a^i) \text{ or } (\hat{\varepsilon}_a^i < \varepsilon^i < \varepsilon_a^i) \text{ and } \left(\text{flag}^{(k-1)} \neq c\right); \\ \sigma^{(d,i)} = \sigma_a^i + k_{h+}^i(\varepsilon^i - \varepsilon_a^i), \text{ for } (\varepsilon_a^i \leq \varepsilon^i \leq \hat{\varepsilon}_c^i) \text{ and } \left(\text{flag}^{(k-1)} = a\right); \\ \sigma^{(e,i)} = \sigma_a^i + \Delta\sigma^i + k_{h-}^i(\varepsilon^i - \bar{\varepsilon}_c^i), \text{ for } (\hat{\varepsilon}_a^i \leq \varepsilon^i \leq \bar{\varepsilon}_c^i) \text{ and } \left(\text{flag}^{(k-1)} = c\right); \\ \sigma^{(c,i)} = k_c^i(\varepsilon^i - \varepsilon_*^i)/\left(1-(\varepsilon^i - \varepsilon_*^i)\right), \text{ for } (\varepsilon^i > \hat{\varepsilon}_c^i) \text{ or } (\bar{\varepsilon}_c^i < \varepsilon^i < \hat{\varepsilon}_c^i) \text{ and } \left(\text{flag}^{(k-1)} \neq a\right). \end{cases} \tag{7.2}$$

Here σ^i is the stress and at each time step $t=t_k$ *(k=1.... M)* and,

$$\text{flag}^{(k)} = \begin{cases} a, \text{ if } \sigma^i = \sigma^{(a,i)} \\ c, \text{ if } \sigma^i = \sigma^{(c,i)} \\ \text{flag}^{(k-1)}, \text{ otherwise.} \end{cases} \tag{7.3}$$

The constitutive parameters $k_0^i, k_c^i, \Delta\sigma^i, \varepsilon_a^i, \varepsilon_c^i, k_{h+}^i$ and k_{h-}^i in Eq. (7.2) are seven independent quantities, while $\hat{\varepsilon}_a^i$ and $\hat{\varepsilon}_c^i$ are computed by solving the following equations (7.4) and (7.5) for ε^i, respectively.

$$\sigma^{(a,i)} = \sigma^{(e,i)}, \tag{7.4}$$

$$\sigma^{(c,i)} = \sigma^{(d,i)}. \tag{7.5}$$

The stiffness parameters k_0^i and k_c^i represent the initial slopes $d\sigma^i/d\varepsilon^i$ at $\sigma^i = 0$, of the bilateral branches OA_1 and C_1C_2 (Figure 7.1). These two branches represent the initial elastic regime and the final densification regime of each spring, respectively. The k_{h+}^i is the slope of the unilateral branch A_1C_1, describing the snap buckling and the consequent hardening during the loading phase. The k_{h-}^i is the slope of the unilateral branch C_2A_2, describing the snap-back recovery of the buckles during unloading phase. When k_{h+}^i and k_{h-}^i are zero, the unilateral branches describe a perfectly plastic behavior. The $\Delta\sigma^i$ equals to the $\bar{\sigma}_c^i - \sigma_a^i$, where the σ_a^i and $\bar{\sigma}_c^i$ are the stresses corresponding to the points A_1 and C_2.

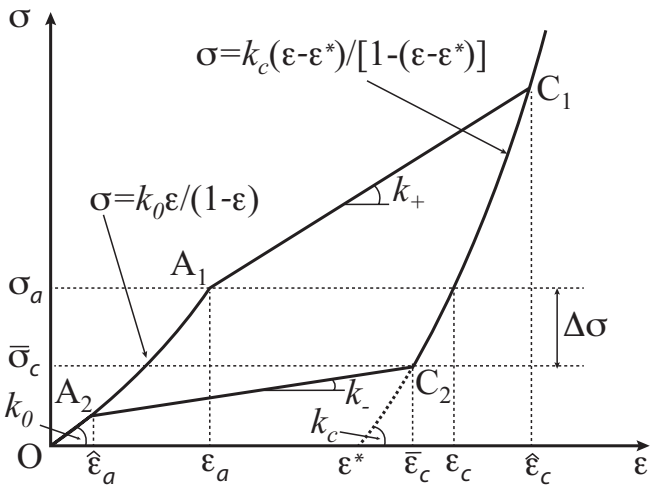

Figure 7.1. Schematic diagram showing the response of a generic mesoscopic dissipative spring element and the relevant constitutive parameters.

This model does not allow for the accumulation of permanent strains that is often found in the compression experiments of VACNT foams, both in their quasistatic [37] and dynamic [166] responses. However, it can be modified to prevent snap-back recovery of springs and allow permanent damage [200]. Similarly, the model can be generalized to describe preconditioning effects found in cyclic loading by introducing initial strains, $\varepsilon_0^i \geq 0$, and elastic strains, $\underline{\varepsilon}^i = \varepsilon^i - \varepsilon_0^i$, for each spring as described in [199]. In this chapter, we will not attempt to extend these features in dynamics.

7.4 Experimental fit and *in-situ* parameter identification

We model the striker as a rigid particle with lumped mass equal to the mass of the striker (7 g) and the force sensor as a rigid fixed wall (Figures 7.2 (a) and (b)). We apply the experimental stress-time history to the particle that represents the striker (top particle), and determine the stress-time and the displacement-time histories at the base of the VACNT foam (force sensor side) using the numerical model described in the previous section. The whole sample is assumed to be in dynamic equilibrium throughout the duration of the experiment [169].

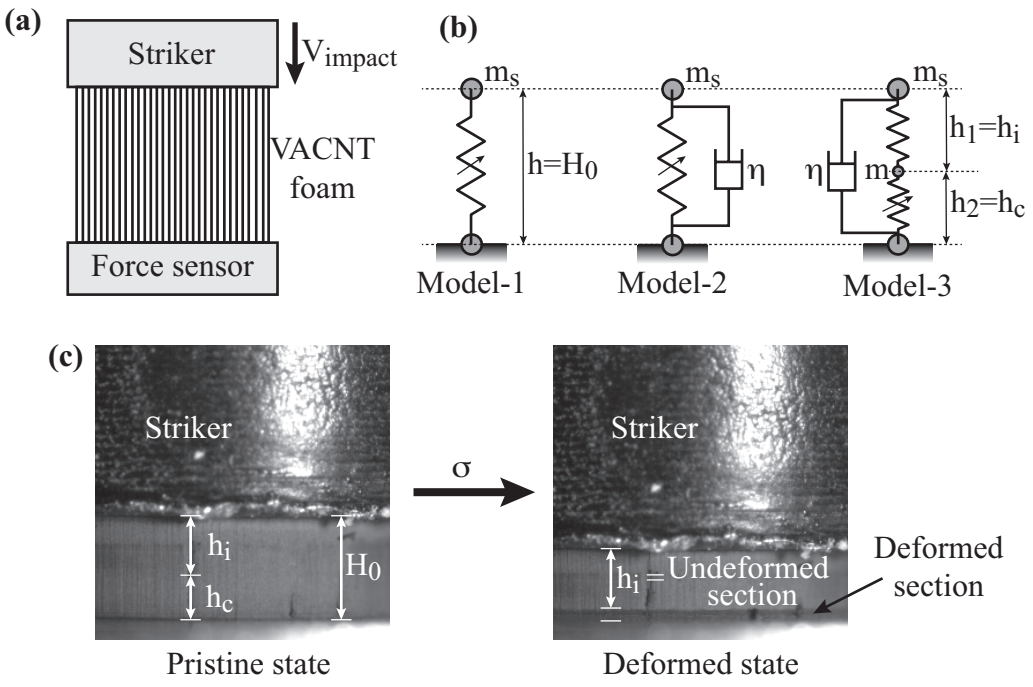

Figure 7.2. Description of the model for the sample impacted at 1.75 m s^{-1}. **(a)** Schematic of the experiment showing the sample being compressed by the striker against the rigidly mounted force sensor. **(b)** Three different models considered for the sample. **(c)** Optical images showing the pristine and deformed states of the sample. Markers are used to highlight the deformed and undeformed sections of the sample.

Figure 7.2 (c) shows selected snap shots obtained from the high-speed image sequence, corresponding to the pristine state of the VACNT foam-1 at the instance of impact ($V_{striker}$=1.75 m s^{-1}) and the deformed state at maximum compression ($V_{striker}$=0). A visualization of the dynamic deformation of the sample can be found in Supplementary Video 3.1. As shown on Figure 7.2 (c), collective buckles nucleate at the bottom of the sample during impact and progressively compress the sample to the height of h_c=0.490 mm. The remaining section of the sample with height, h_i=0.700 mm undergoes infinitesimal compressive strains. As a first approximation (Model-1 in Figure 7.2(b)), we represent the whole height (1.190 mm) of the sample as a single effective spring (macroscopic dissipative element) that connects the striker particle to the rigid wall (force sensor). In addition, we neglect the mass of the VACNT foam (5.56 mg) in comparison to the large striker mass (7 g). The seven independent parameters that define the nonlinear

spring of Model-1 are listed in Table 7.2. Figure 7.3 (a) (top panel) shows the stress- and displacement-time histories and the stress-strain diagram obtained with Model-1 (and superimposed to the experimental data). The overall results show a good agreement with experiments. The time histories of stress and displacement, however, exhibit significant oscillations that arise from numerical instabilities. These instabilities are particularly evident when the model transitions between adjacent branches of the dissipative spring element—for example, see the inset of stress-time history in Figure 7.3 (a).

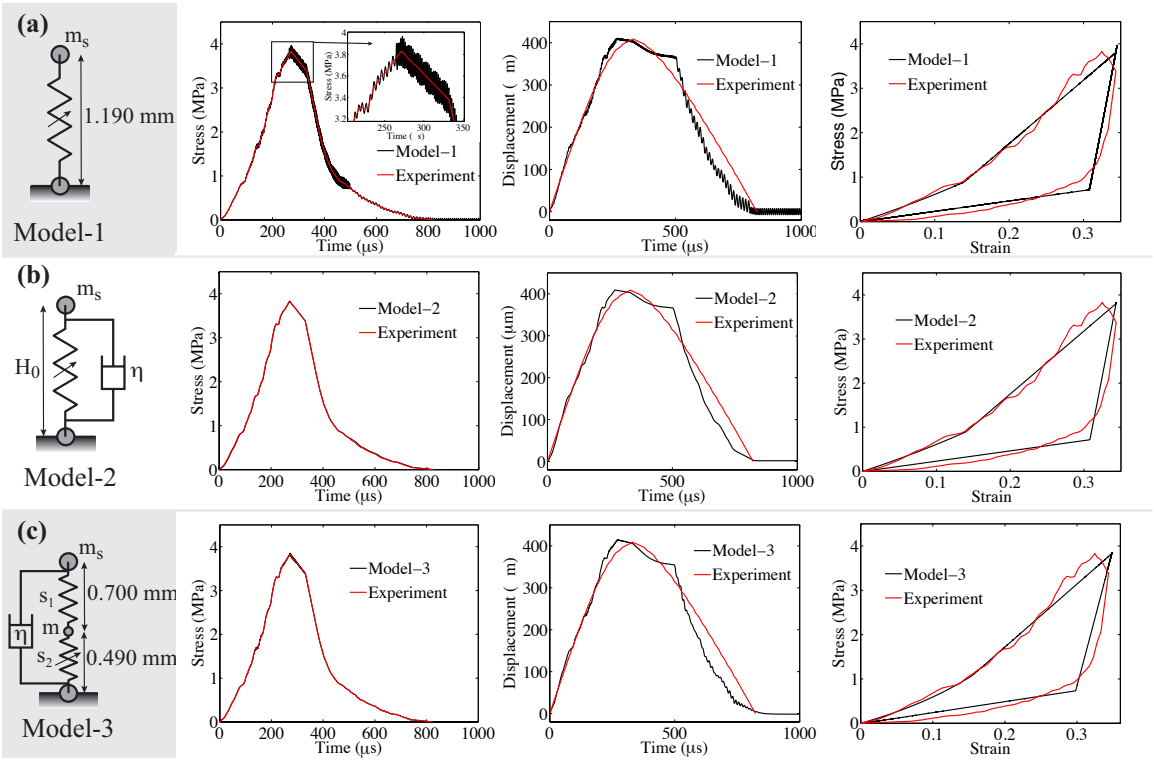

Figure 7.3. Comparison of the numerical and experimental results of stress-time histories, displacement-time histories and stress-strain responses for **(a)** Model-1, **(b)** Model-2 and **(c)** Model-3 of the VACNT foam-1.

To ensure stability during the dynamic transitions between phases, we introduced an onsite damper with damping coefficient 0.01 MPa s to the striker mass (Model-2 in Figure 7.2 (b)). The damping ratio between the adopted damping coefficient and the critical damping coefficient associated with the unloading branch ($2h\sqrt{\rho k_c}$) is calculated to be 0.894. As shown in the middle panel of Figure 7.3 (b), the damper

reduces the numerical instabilities significantly and facilitates smooth dynamic transitions.

Table 7.2. Parameters of the models of VACNT foam-1.

(The definition of these parameters is shown in Figure 7.3. In Model-3, S1 is the linear spring and S2 is the nonlinear, bi-stable spring.)

		k_0 (MPa)	$\Delta\sigma/\sigma_a$	η (Pa.s)	ϵ_a	ϵ_c	h (mm)	k_{h+}/k_0	k_{h-}/k_0	k_c/k_0
Model-1		5.50	-0.20	-	0.14	0.31	1.190	2.60	0.450	15
Model-2		5.50	-0.20	$1x10^4$	0.14	0.31	1.190	2.60	0.425	15
Mod el-3	S1	60	-	$3\ x10^2$	-	-	0.700	-	-	-
	S2	2	-0.32		0.35	0.71	0.490	3.40	0.525	30

We refine the model further to account for the elastic properties of the deformed section of the CNT foams (Model-3). The refined model employs a dissipative spring element (S_2,), with height h_2=0.490 mm, to describe the response of the heavily deformed (or "buckled") section of the sample, and models the section of the sample that undergoes infinitesimal strains through a linear spring (S_1) with height h_1=0.700 mm (Figure 7.2 (b)). We set the stiffness of this linear spring to be approximately equal to the unloading stiffness (k_c) of the nonlinear spring, in order to localize the deformation in S_2. We introduce another lumped mass equal to the mass of the VACNT foam sample (5.56 mg) in between these two springs. The bottom panel of Figure 7.3 (c) shows that the numerically obtained global dynamic response of the sample is in good agreement with experiments. As shown in the parameters listed in Table 7.2, the nonlinear spring (S_2) of Model-3 exhibits lower initial stiffness (k_0) compared to that in Model-2, since it identifies specifically the buckled region as an effective spring. Also, due to the snap-buckle and the consequent densification in spring S_2, the unloading stiffness parameter k_c

shows a higher value compared to that of Model-2. The damping ratio required for ensuring the numerical stability of Model-3 is 0.0297 (significantly less than the same value in Model-2).

We apply a similar two-spring model to the VACNT foam-2 that was impacted at 4.44 m s^{-1} (Figure 7.4). In a similar manner to the previous case, we use a dissipative element as an effective spring for the buckled section of the sample (h_2=0.756 mm) and represent the infinitesimally strained section (h_1=0.350 mm) with a unilateral linear spring. An onsite damper with damping coefficient of 1 x 10^4 is used to ensure stability during numerical simulation. The damping ratio required for such numerical stability is 0.525.

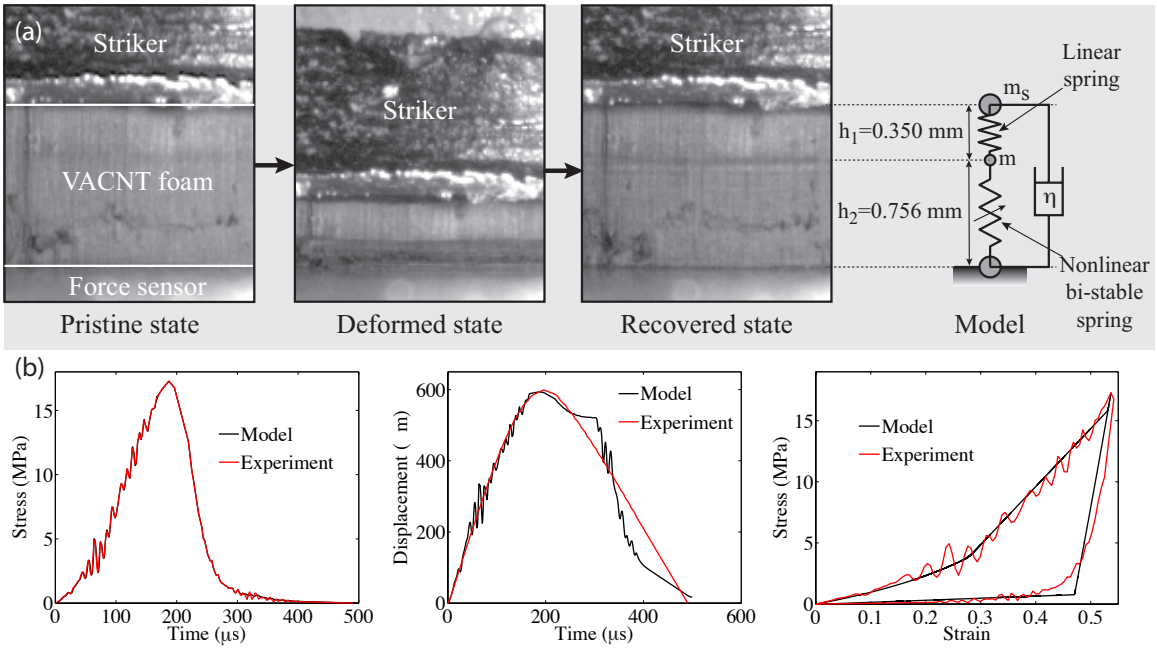

Figure 7.4. (a) Optical images selected from the high-speed camera sequence showing the sample VACNT foam-2 before the impact (pristine state), at its maximum deformation (deformed state) and after load release (recovered state) [169]. The schematic diagram on the right shows the model employed and its relevant parameters. This sample was impacted at 4.44 m s^{-1}. **(b)** Comparison of the numerical and experimental results for the stress-time history, displacement-time history and stress-strain response.

Figure 7.4 (b) shows the comparison of numerical and experimental results. The model captures the global dynamics, while identifying the constitutive parameters at a lower

length-scale compared to the sample height (Table 7.3). It should be noted that the sample impacted at high velocity deforms more and reaches higher maximum strain, as compared to VACNT foam-1. Since the height of the nonlinear spring (S_2) describing the buckled region is significantly higher in VACNT foam-2 than in VACNT foam-1, the stiffness constant k_0 of VACNT foam-2 (5.75 MPa) is appreciably higher than k_0 of VACNT foam-1 (2.00 MPa). This increase in stiffness is explained by the increase in the intrinsic density of CNTs along the height [166].

Table 7.3. Parameters of the model of VACNT foam-2.

(The definitions of these parameters are shown on the Figure 7.3. S1 is the linear spring and S2 is the nonlinear bi-stable spring.)

	k_0 (MPa)	$\Delta\sigma/\sigma_a$	η (Pa.s)	ϵ_a	ϵ_c	h (mm)	k_{h+}/k_0	k_{h-}/k_0	k_c/k_0
S1	250	-	1×10^4	-	-	0.350	-	-	-
S2	5.75	-0.80		0.40	0.70	0.756	6.00	0.200	40

7.5 Conclusions

We introduced phenomenological models to describe the dynamic response of VACNT foams under high-rate compression. The models use a one-dimensional mass-spring system containing an effective dissipative spring element, which describes either the entire sample (single-spring model), or its buckled (heavily deformed) section (two-spring model). We have shown that the models allow us to characterize the bulk dynamic response of the VACNT foams and their dissipation properties. The adopted spring models employ the concept of rate-independent, transformational plasticity, as opposed to more conventional, rate-dependent and/or plastic models. We have also introduced numerical viscosity through the phenomenological approach proposed in [201]. The two-

spring model enables the identification of the VACNT foams' mechanical parameters, at length-scales smaller than the sample height.